Temperature-induced valence instability in the charge-transfer crystal TMB-TCNQ

Nicola Castagnetti,[1] Gabriele Kociok-Köhn,[2] Enrico Da Como,[3] and Alberto Girlando[1,*]

[1]*Dipartimento di Chimica and INSTM-UdR Parma, Università di Parma, Parco Area delle Scienze 17/a, I-43124 Parma, Italy*

[2]*Chemical Characterisation and Analysis Facility (CCAF), University of Bath, Claverton Down, Bath BA2 7AY, United Kingdom*

[3]*Department of Physics, University of Bath, Claverton Down, Bath BA2 7AY, United Kingdom*

(Received 1 October 2016; published 3 January 2017)

The occurrence of so-called temperature-induced neutral-ionic transitions (TINIT) in mixed-stack charge-transfer crystals is quite rare. Here we reinvestigate one of the crystals which has been claimed to undergo such a transition, 3,3′,5,5′-tetramethylbenzidine-tetracyanoquinodimethane (TMB-TCNQ). Extensive optical data allow us to conclude that the transition should be classified as a valence instability, and not as a "true" TINIT, as the ∼0.5 neutral-ionic borderline is not crossed. The ionicity ϱ, or average charge at the molecular sites, indeed changes very little at the transition, from about 0.3 to about 0.4, and is accompanied by stack dimerization. The transition is first order with large hysteresis, and the crystal may crack or break. For this reason we have been unable to collect x-ray structural data on the low-temperature phase, but with the help of semiempirical calculations we are able to assess a plausible scenario for this peculiar phase transition and its mechanism.

DOI: 10.1103/PhysRevB.95.024101

I. INTRODUCTION

Organic charge-transfer (CT) crystals made up by π electron-donor (D) and electron acceptor (A) molecules arranged alternatively in a typical $\cdots$DADAD$\cdots$ mixed-stack structure may undergo a rather unique phase transition, the so-called neutral-ionic phase transition (NIT) [1,2]. The NIT implies a *collective* CT from D to A, with the average charge at the molecular site, or ionicity ϱ, crossing the N-I borderline conventionally placed at $\varrho = 0.5$ [3]. It was recognized early that mixed-stack CT crystals are also subject to Peierls instability, yielding stack dimerization $\cdots$DA DA DA$\cdots$ [4]. Peierls dimerization may occur at the same time as the ionicity change [4] or independently [5]. In fact, on the ionic side a regular stack is intrinsically unstable towards dimerization (degenerate ground state), whereas in the proximity of the N-I borderline ($\varrho \geqslant 0.3$–0.4) the instability is conditional, i.e., depends on the strength of the electron-lattice phonon coupling [6]. The competition between two instabilities: a first-order one, driven by the three-dimensional Madelung energy (valence instability; order parameter, ϱ); and a second-order one, driven by electron-lattice phonon coupling (Peierls instability; order parameter, stack dimerization) makes the NIT a complex and intriguing phenomenon.

Since its discovery more than 30 years ago, the temperature-induced NIT, or TINIT [2], has been extensively studied in view of the many fascinating phenomena (dielectric anomaly, quantum phase transitions, ferroelectricity, overdamped Peierls mode, divergent polarizability, etc.) associated with it [7–9]. Yet only a handful of mixed CT crystals have been shown to undergo TINIT, in addition to the prototypical tetrathiafulvalene-chloranil (TTF-CA) [10,11]. Among them, 3,3′,5,5′-tetramethylbenzidine-tetracyanoquinodimethane (TMB-TCNQ) has been claimed to undergo TINIT at $T \approx 200$ K, with large hysteresis and with a ϱ change of about 0.1 just around the N-I borderline [12]. Despite the many similarities to TTF-CA and the convenient high temperature of the transition, no further investigation has been performed, except for a study on thermal hysteresis, where it was shown that the crystals break at the transition [13]. We have thus decided to reinvestigate this system, to understand better the nature and the mechanism of the phase transition, and to try to characterize the low-temperature phase.

II. EXPERIMENTAL PROCEDURE

A. Sample preparation

TMB-TCNQ crystals were obtained both by precipitation from solution and by sublimation in a closed ampoule. By mixing saturated solutions of the two components in hot acetonitrile, followed by slow cooling and solvent evaporation, we obtained crystals with a high degree of disorder, which could not be characterized by x ray. These crystals did not show phase transitions down to 77 K, and likely belong to the early-reported triclinic phase [14,15]. Good crystals were obtained from solution by following a different procedure: 5 ml of a TMB-saturated solution in isopropylic alcohol was carefully layered onto 5 ml of a TCNQ-saturated solution in dichlorobenzene-chloroform [1:1], in a 10-ml closed tube. The alcoholic TMB solution stands on the more dense and viscous TCNQ solution and promotes slow diffusion of the solutes at the interface, yielding the formation of crystals. After 3 days it was possible to observe needle-shaped crystals of millimetric size at the interface between the two liquids. After 1 week the solution was filtered and the crystals were collected.

In sublimation growth, powders of the starting materials TMB and TCNQ were put in a clean glass ampoule. The ampoule was sealed by flame while being kept under low vacuum, $\sim 10^{-3}$ mb (rotative pump). Then the ampoule was inserted into a two-heating-zone tubular furnace for growth. The furnace was set to a proper temperature profile, i.e., around 195°C at the source and around 160°C in the colder deposition area. The ampoule was kept at this temperature for 1 week, and formation of needle-shaped crystals was observed in the cold area.

*girlando@unipr.it

The needle-shaped crystals grown by vapor phase are of good quality, with well-formed surfaces. Crystals grown by solution instead tend to be twinned, always with a needle shape, but they are thinner than the sublimation-grown crystals. The crystal structure is the same and coincides with that reported by Iwasa *et al.* [12].

B. Instrumentation

Single-crystal diffraction intensity data for all structures were collected at 230 K on an Agilent SuperNova-E Dual diffractometer equipped with an Oxford Cryosystem, using CuK radiation ($\lambda = 1.5418$ Å). Data were processed using the CrysAlisPro software [16].

Infrared (IR) spectra were recorded with a Bruker IFS66 Fourier transform IR (FT-IR) spectrometer coupled to the Hyperion 1000 IR microscope. The instrument setup allows for reflection and transmission measurements with polarized light, and we used both techniques, depending on the crystal thickness and surface quality. The Raman spectra, excited with the 647-nm line of a Lexel Kr laser, were recorded with a Renishaw 1000 Raman spectrometer, equipped with the appropriate edge filter, and coupled to a Leica M microscope. A small liquid nitrogen cryostat (Linkam HFS 91) was used for low-temperature optical measurements under the microscopes.

C. Computational methods

Standard density functional methods [GAMESS package [17], B3LYP functional, 6-31G(d) basis set] were used for the equilibrium geometry and molecular vibrations of the isolated neutral and ionized TMB molecule. We instead used a semiempirical approach (MOPAC16 package [18], PM7 parametrization) for calculation of the equilibrium structure of the TMB-TCNQ crystal.

III. RESULTS

A. Single-crystal x-ray structure

Our x-ray diffraction measurements, collected at 230 K, confirm the previously reported room-temperature crystal structure [12]: monoclinic space group $P2_1/n$ (C_{2h}^5), with lattice constants $a = 6.708(3)$ Å, $b = 21.797(7)$ Å, $c = 8.074(3)$ Å, $\beta = 100.35(5)$, $Z = 2$ ($R = 4.03$). TMB and TCNQ molecules reside on inversion centers and are stacked along the a axis, with an interplanar distance of 3.35 Å. A projection of the unit cell along the stack axis is shown in Fig. 1, illustrating the good overlap between the frontier orbitals of the two molecules [19]. Also note that the DADAD order of the two stacks in the unit cell is staggered, so that in the layers parallel to the bc planes each A molecule has four nearest-neighbor D molecules, and vice versa.

The bond distances of TCNQ have been widely used to estimate the ionicity ϱ in charge-transfer crystals [20,21]. The method essentially assumes a linear relationship between the ionicity and the ratio $\alpha = c/(b + d)$, where b, c, and d are the TCNQ ring CC single bond and the "wing" C=C and C-C bonds, respectively. From our structural data $\alpha = 0.4813$, and following the calibration in Ref. [21], we obtain $\varrho = 0.25$, much lower than the early estimate from IR data [12].

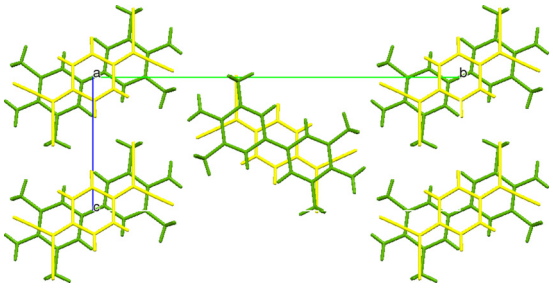

FIG. 1. View of the TMB-TCNQ unit cell along the a stack axis. TMB and TCNQ molecules are shown in green and yellow, respectively, to illustrate the overlap between the two molecular structures.

B. Room-temperature infrared and Raman spectra

In their optical characterization of TMB-TCNQ, Iwasa *et al.* [12] have reported polarized reflectance spectra in the 2160–2230 cm^{-1} region, where CN stretching vibrations occur, and the visible region, where intramolecular excitons are present. Here we extend the polarized IR data to the full mid-IR vibrational region and to the near-IR, i.e., the region of the CT transition. Furthermore, we also present the Raman spectra.

The room-temperature mid-IR polarized absorption spectra are reported in Fig. 2. The examined plane contains the a stack axis and is likely the ac one. The spectra were recorded with the electric-field vector perpendicular to the stack (red curve in Fig. 2), showing the vibrational motions in the plane of the molecules, and with the electric-field vector parallel to the stack (black line in Fig. 2), where out-of-plane motions are detected.

The charge-sensitive vibrations of TCNQ, namely, the CN stretching $b_{1u}\nu_{19}$ and the C=C stretching $b_{1u}\nu_{20}$ [22], are clearly visible in the perpendicular spectra. We remark that three absorptions are observed in the CN stretching region (Fig. 2, right), at 2204, 2176, and 2156 cm^{-1}, whereas only two are expected. $b_{1u}\nu_{19}$ corresponds to the highest frequency and gives $\varrho = 0.49$, a value similar to that reported in Ref. [12]

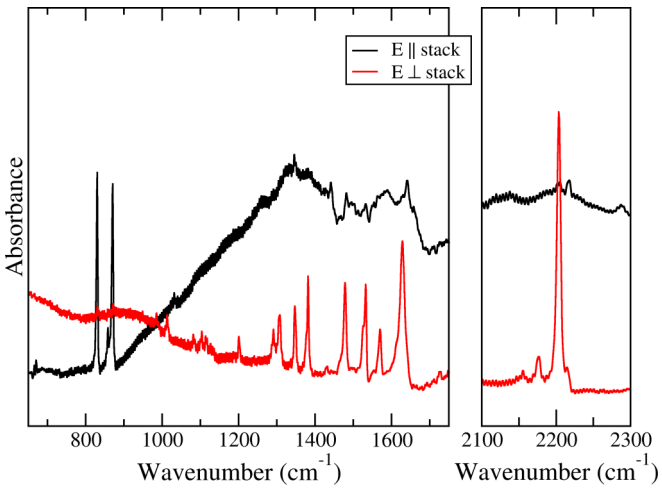

FIG. 2. Polarized mid-IR spectra of TMB-TCNQ at room temperature. The different polarizations are offset for clarity.

on the basis of reflectance spectra, but not consistent with the above estimate from the structural data. On the other hand, it is well known that the TCNQ $b_{1u}\nu_{19}$ CN stretching frequency gives unreliable (generally overestimated) values of ϱ since it suffers from uncertainty about the correct assignment and is subject to extrinsic effects due to the interactions with the surrounding molecules [23,24]. For this reason we extended the investigated range to the spectral region where $b_{1u}\nu_{20}$ C=C stretching occurs. The frequency of this mode indeed gives a much more reliable estimate of ϱ and, in the present case, is also easily identified, since it occurs in a spectral region (1550–1500 cm^{-1}) completely free of absorptions of the TMB unit [19]. From this absorption, occurring at 1532 cm^{-1}, we obtain $\varrho = 0.29$, a value quite consistent with the value estimated from the x-ray TCNQ bond lengths.

The out-of-plane modes are active in the parallel polarization (black curve in Fig. 2), and indeed two bands, at 870 and 830 cm^{-1}, are clearly identified as due to the TMB $a_u\nu_{87}$ and TCNQ $b_{3u}\nu_{50}$ modes, respectively. Between 1000 and 1600 cm^{-1} the parallel spectrum presents a very broad band, with a strange shape. The increase in the baseline is due to the proximity of the onset of the very intense CT electronic transition, also polarized along the stack axis (see below). On the other hand, the very strange and complex band shape can be explained by considering that, as in TTF-CA [25], we are in the presence of combination modes between the Raman active, totally symmetric intramolecular modes and the low-frequency intermolecular Peierls mode(s). All these modes are coupled together through the CT electron. In TTF-CA, these modes could be identified, since the totally symmetric modes coupled to the CT electron are relatively few and isolated. In the present case between 1000 and 1600 cm^{-1} we have instead many strongly coupled totally symmetric modes, from both TMB and TCNQ, so that the combination modes overlap and coalesce, giving rise to the strange band shape.

As mentioned, the CT electronic transition, polarized along the stack axis, saturates the absorption spectrum. Therefore we have collected the near-IR parallel spectrum in specular reflectance. The result is reported in Fig. 3, together with the corresponding conductivity spectrum obtained by Kramers-Kronig transformation. The peak frequency in the conductivity spectrum is 7560 cm^{-1}, or 0.94 eV. Fitting the conductivity with a Lorentzian line shape and with the unit cell density derived from the crystallographic data, we estimate the oscillator strength of the CT band as $f_{CT} = 0.58$. Using the calculations in Ref. [26], we estimate $\varrho \simeq 0.28$, and the hopping integral $t \simeq 0.4$ eV, about twice that of TTF-CA, as expected given the better overlap between the frontier orbitals of the donor and acceptor molecules.

Figure 4 reports the room-temperature Raman spectrum of TMB-TCNQ in the spectral region of intramolecular vibrations. Only one polarization is reported (electric vector of incident and scattered light perpendicular to the stack axis), as no additional information is provided by the other polarizations. The spectra are dominated by the TCNQ totally symmetric vibrations, as these have a very high Raman cross section. We also remark that two bands of comparable intensity are present in the CN stretching region. Since the CN stretching of b_{3g} symmetry has an intensity much lower than that of the corresponding a_g mode [27], we attribute the doublet structure

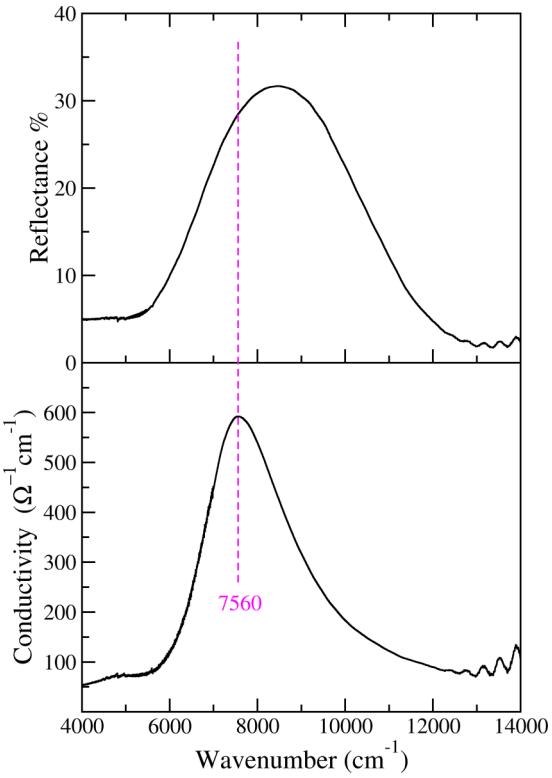

FIG. 3. Near-IR spectrum of TMB-TCNQ; polarization along the stack axis. Top: Reflectance spectrum. Bottom: Conductivity spectrum obtained by Kramers-Kronig transformation.

to the effect of different crystalline environments for the CN groups, as is likely the case for the three bands observed in the IR.

The TCNQ $a_g\nu_4$ mode, located at 1454 cm^{-1} in neutral TCNQ [27] and exhibiting an ionization frequency shift Δ of 63 cm^{-1} [22], has often been used to estimate the ionicity of segregated-stack CT crystals like TTF-TCNQ [28]. However, totally symmetric modes are coupled to the CT electron

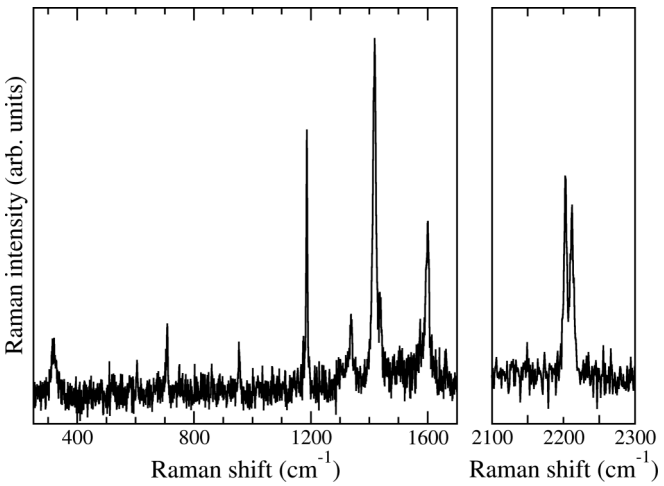

FIG. 4. Raman spectrum of TMB-TCNQ at room temperature with the electric vector of the incident and scattered light perpendicular to the stack axis.

(e-mv interaction) [29], and in mixed-stack crystals the linear dependence of their frequency from ϱ is lost. Nevertheless, a rough estimate of ϱ can be obtained by taking into account the perturbing effect of e-mv interaction through an appropriate model. For a regular chain like room-temperature TMB-TCNQ we can use the trimer model, and by disregarding the interaction among e-mv coupled modes (isolated band approximation), the perturbed frequency Ω is given by [30]

$$\Omega = \sqrt{(\omega_0 - \Delta\varrho)\left[(\omega_0 - \Delta\varrho) - \frac{4g^2}{\omega_{CT}}\varrho(1-\varrho)^2\right]}, \qquad (1)$$

where ω_0 is the vibrational frequency of the neutral molecule, Δ the ionization frequency shift, g the e-mv coupling constant, and ω_{CT} the frequency of the CT transition. In TMB-TCNQ the $a_g\nu_4$ mode occurs at 1418 cm^{-1}, $\omega_{CT} = 7560$ cm^{-1}, and with a value of 65 meV for the e-mv coupling constant of the $a_g\nu_4$ mode [29] Eq. (1) gives $\varrho \approx 0.4$. Being model dependent, this estimate is very approximate and just gives a consistency check of the values obtained by other methods.

To summarize, the x-ray bond distances and the analysis of the CT transition and of the charge-sensitive vibrations (except for the unreliable CN stretching mode) all place room-temperature TMB-TCNQ well on the neutral side, with ϱ between 0.25 and 0.30. In the following we refer to the value obtained from the $b_{1u}\nu_{20}$, $\varrho = 0.29$, since we can use only this method to estimate the degree of charge transfer below the phase transition.

C. The phase transition

From the analysis in the previous sections, it turns out that at room temperature TMB-TCNQ is very similar to TTF-CA [31] or to dimethyltetrathiafulvalene-chloranil (DMTTF-CA) [32] just above the neutral-ionic phase transition: ionicity not far from the N-I borderline, CT transition in the IR frequency range, and evidence of the low-frequency Peierls(s) mode by the so-called IR "sidebands" in the parallel IR spectra.

We first collected structural data at 150 K, well below the reported transition temperature of 205 K [12], but the refinement gave a $P2_1/n$ structure, the same as that collected at 230 K, although with a worse R factor (7.89). The extensive spectroscopic measurements we have collected show that the occurrence of the transition and its critical temperature are scarcely reproducible [13], particularly if the sample is embedded or put in contact with different substrates, e.g., a KBr window or Nujol mull. The cooling rate does not seem to be important, and the sample often breaks at the transition [13]. In the case of x rays it is likely that the grease used to hold the sample prevents the phase transition, although microcrackings will worsen the refinement. Actually, the reported transition temperatures of ≈205 K upon cooling and of ≈235 K upon heating could be obtained only for "free" samples, for instance, a crystal leaning on a glass slide. Also, simple grinding of the crystal may prevent the transition down to 77 K.

In order to avoid confusion by referring to the critical temperatures, henceforth we refer to the phases above and below the transition as the high-temperature (HT) and low-temperature (LT) phases, respectively.

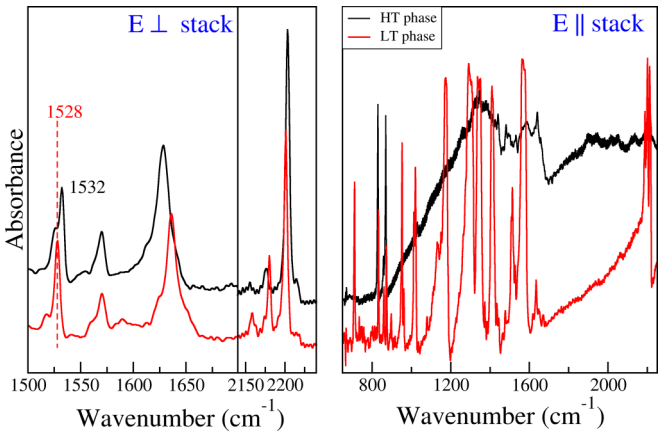

FIG. 5. Infrared spectrum of TMB-TCNQ above (HT phase) and below (LT phase) the transition temperature. The spectra of the two phases are offset for clarity.

Breaking or cracking of the sample does not prevent the collection of good-quality absorption and Raman spectra under the microscope. Figure 5 compares the polarized IR absorption spectra above and below the phase transition in the spectral regions of interest. The spectra polarized perpendicular to the stack (left) show that the charge-sensitive bands shift very little with the transition. In particular, the $b_{1u}\nu_{20}$ C=C stretching moves from 1532 to 1528 cm^{-1}, which corresponds to a ϱ increase of about 0.1, from 0.29 to 0.41. The absolute value of the ionicity is not reliably estimated from the CN stretching, but the relative change obtained from the frequency lowering is $\Delta\varrho = 0.1$, as from the C=C stretching. Therefore TMB-TCNQ remains on the neutral side also in the LT phase. On the other hand, the appearance of very strong bands in the spectra polarized parallel to the stack (Fig. 5, right) as in the TTF-CA low-temperature phase [4] unambiguously demonstrates that the stack dimerizes at the transition [29]. These bands are in fact associated with the e-mv coupled totally symmetric Raman active modes, which become IR active due to the loss of the inversion center and borrow intensity from the nearby CT transition. We note that they are more numerous than those observed in the Raman spectra (Fig. 2 and Fig. 6). The reason is that, as already mentioned, the Raman spectra are dominated by the TCNQ bands, whereas the e-mv-induced bands are due to both the TCNQ and the TMB totally symmetric modes with appreciable values of the e-mv coupling constants.

Figure 6 shows that the frequency of the TCNQ $a_g\nu_4$ mode decreases by 7 cm^{-1} upon going from the HT to the LT phase. As already mentioned, the estimate of ϱ from Raman is very approximate in the present case. For the LT phase, the use of the dimer model [29,30] with the further assumption of an unshifted CT band (we could not record the reflectance spectrum in the LT phase due to the surface damage at the transition) gives practically the same $\varrho \approx 0.4$ as the HT phase. The Raman data essentially confirm that the N-I borderline is not crossed at the transition.

Finally, Fig. 7 compares the low-frequency Raman spectra of HT and LT phases. The lattice modes occurring in this spectral region are very sensitive to the crystal structure and packing [33]. In this case we present both the (⊥⊥) and the

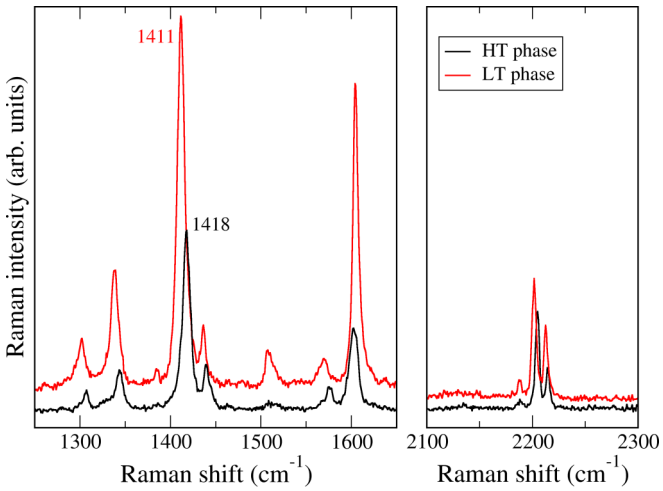

FIG. 6. Raman spectrum of TMB-TCNQ above (HT phase) and below (LT phase) the transition temperature. The electric vector of the incident and scattered light is perpendicular to the stack axis. The spectra of the two phases are offset for clarity.

($\parallel\perp$) polarizations ($\perp$ and $\parallel$ with reference to the stack axis). In the examined ac plane of the HT phase, we expect three Raman totally symmetric lattice modes to be present in the two polarizations with possibly different intensities, and indeed we detect three bands, at 39, 51, and 69 cm^{-1}. In the LT phase twice the number of bands is observed, at 35, 42, 50, 60, 79, and 128 cm^{-1}, clearly indicating a symmetry lowering of the unit cell. This finding is consistent with the above-discussed appearance of e-mv-induced bands in the LT-phase IR spectra, which indicates dimerization of the stack, i.e., loss of the inversion center. A minimum loss of symmetry implies the passage from a C_{2h} factor group to either a C_s group, like TTF-CA [34], or a C_2 group.

To summarize the discussion up to this point, the first-order transition of TMB-TCNQ implies a change of ionicity $\Delta\rho \simeq$ 0.1, from 0.29 to 0.41, and is accompanied by dimerization of the stack. As in the case of DMTTF-CA [32], the phase transition can hardly be considered a "true" NIT, since the $\rho \simeq 0.5$ borderline is not crossed but, rather, a (small) valence instability. But in the present case we have a first-order transition, as in TTF-CA, with crystal cracking or breaking and large hysteresis, whereas for DMTTF-CA the transition is practically continuous. From this point of view, the TMB-TCNQ transition appears to be different from the other known transitions of 1:1 mixed-stack CT crystals. We finally remark that even if the N-I borderline is not crossed, the TMB-TCNQ LT phase is potentially ferroelectric, since the stack is dimerized and has an intermediate degree of charge transfer. Ferroelectricity will be observed if the two stacks in the unit cell present in-phase dimerization, like TTF-CA [34].

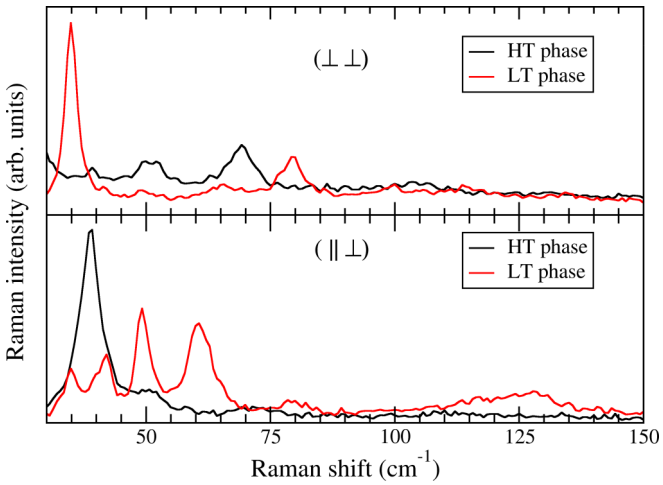

FIG. 7. Low-frequency polarized Raman spectrum of TMB-TCNQ above (HT phase) and below (LT phase) the transition temperature. The $\perp$ and $\parallel$ symbols indicate the orientation of the electric vector of incident and scattered light with respect to the stack axis.

The cracking of the sample and the lack of reproducibility prevent us from getting structural information on the LT phase. We then adopted a computational approach to get some hint about the type of interaction triggering the transition and the associated mechanism. Since DFT calculations on the free TMB molecule have shown that the equilibrium conformation is different from the experimental one inside the crystal [19], we need a computational approach allowing for the unit cell change/symmetry breaking *and* for the relaxation of the molecular conformation. DFT methods are computationally very demanding for the above task, and the results also depend on the chosen functional and basis set [35]. Furthermore they are not guaranteed to give results better than those with the by far simpler atom-atom potentials [36]. In this particular case, we chose a semiempirical calculation, MOPAC16 with PM7 parametrization, a method widely tested and optimized for equilibrium geometries [18].

Starting from the experimental $P2_1/n$ structure at 230 K and considering four unit cells, the minimum potential equilibrium geometry at 0 K was reached after 668 cycles. All the unit-cell symmetry was apparently lost in the minimum search, but the use of a symmetry-recognition program [37] actually showed that the structure deviates very little from the monoclinic $P2_1$ (C_2^2) space group. A comparison of the cell structure of the experimental HT phase and of the computed LT phase is given in Table I and in Fig. 8.

Table I shows that the symmetry breaking at the phase transition implies the loss of the inversion center, in agreement with the IR measurements, and of the glide plane. The a axis length increases and the c axis decreases, but overall the

TABLE I. Experimental and calculated structural parameters of the TMB-TCNQ HT and LT phases.

	HT phase (expt.)	LT phase (calc.)
Space group	$P2_1/n$	$P2_1$
a (Å)	6.708	6.785
b (Å)	21.797	21.797
c (Å)	8.074	8.068
β (deg)	100.35	100.13
Z	2	2
Cell volume (Å^3)	1161.3	1174.6
D-A distance (Å)	3.35	3.95, 2.81

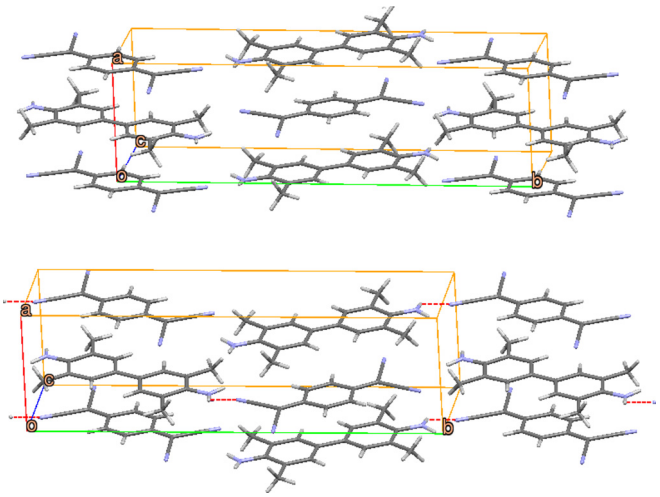

FIG. 8. Crystal packing of TMB-TCNQ. Top: Experimental x-ray structure above the critical temperature. Bottom: Calculated structure below the critical temperature.

cell volume slightly *increases* in the LT phase, which might well explain the crystal breaking. Moreover, the computed expansion and contraction along the a and c axes are consistent with experiment, which indicates that the crystal breaking occurs precisely along these axes [13].

According to the calculations, the increase in the a axis length is due to TMB molecular deformation and H $\cdots$ N interstack contacts between TMB and TCNQ. This is shown in Fig. 8: in the LT phase the apical NH_2 group of TMB deviates markedly from planarity and establishes a closer contact with the N of the TCNQ of the nearby stack (dashed red lines in Fig. 8; the H $\cdots$ N distance varies from 2.186 to 1.588 Å). It is therefore the TMB deformation and H $\cdots$ N contact that trigger the valence instability and the simultaneous stack dimerization, which in the calculations is much larger than in the LT phase of TTF-CA [34]. If we define dimerization as the ratio between the difference and the sum of the DA, AD distances along the stack, we get $\delta_{\text{expt}} = 0.03$ for TTF-CA and $\delta_{\text{calc}} = 0.17$ for TMB-TCNQ. Finally, Fig. 8 also shows that the arrangement of the DA dimers in the unit cell is antiferroelectric.

Of course, one cannot place too much confidence in the results of the calculations, in particular, in the accuracy of the resulting numbers. But the emerging scenario is plausible and fully compatible with the available experimental data.

IV. CONCLUSIONS

The present accurate optical study of TMB-TCNQ has shown that the first-order transition induced by the temperature is better classified as a valence instability rather than a true NIT, as the 0.1 ionicity jump does not lead to a crossing of the N-I borderline. The ionicity jump is accompanied by a strong stack dimerization, and the crystal generally breaks at the transition. The critical temperature ($\approx$205 K upon lowering T and $\approx$235 K upon increasing T) appears to change when the sample is not completely free (e.g., adhesion to the KBr window in the IR measurements) and, possibly, depends also on the sample history. For this reason the transition mechanism is difficult to study. According to our numerical simulation, the TMB-TCNQ transition implies the loss of the inversion center and of the glide plane, yielding to an antiferroelectric arrangement of the DA dimers in the unit cell. Always according to the simulation, the molecular deformation favored by the interstack H $\cdots$ N contacts yields to an increase in the cell volume and appears to be the actual trigger of the transition.

From the present study it turns out that the small number of "true" TINITs is further reduced. As discussed above, the HT phase is very similar to that of TTF-CA or DMTTF-CA just before the transition [31,32]. Yet by lowering the temperature the evolution of the three systems is different: TTF-CA undergoes a discontinuous NIT and DMTTF-CA displays an almost-continuous ionicity change, accompanied by dimerization, but without crossing the N-I borderline. TMB-TCNQ instead has a first-order transition with a discontinuous ionicity change, like TTF-CA, but again without crossing the N-I borderline. To give a rationale for these differences, one has to consider that by increasing the ionicity with lowering T, one reaches a multistability region [38], with competition between a first-order valence instability driven by the three-dimensional Madelung energy and a second-order one-dimensional Peierls instability. At this point very weak intermolecular forces, like weak hydrogen bonding [39] or even van der Waals forces, all connected to the compressibility of the sample, i.e., to the (anisotropic) increase in the Madelung energy, may trigger the transition and drive the system towards one of the possible minima. The weak H $\cdots$ N contacts in this case imply a cell expansion, so that the increase in ionicity due to the Madelung energy is very limited, and the N-I borderline is not crossed. We believe that this complex scenario explains why true TINITs are so rare and why the actual type of phase transition occurring in mixed-stack CT crystals is difficult to predict.

ACKNOWLEDGMENTS

Enlightening discussion with Prof. C. Rizzoli is gratefully acknowledged. This work was supported by Parma University. The work in Bath was supported by the Royal Society through a Wolfson Refurbishment Grant and by the European Union (EU) Horizon2020 research and innovation programme under Grant Agreement No. 646176 (EXTMOS).

[1] J. B. Torrance, J. E. Vazquez, J. J. Mayerle, and V. Y. Lee, Phys. Rev. Lett. **46**, 253 (1981).

[2] J. B. Torrance, A. Girlando, J. J. Mayerle, J. I. Crowley, V. Y. Lee, P. Batail, and S. J. LaPlaca, Phys. Rev. Lett. **47**, 1747 (1981).

[3] We speak of a "conventional" N-I borderline, since a clear distinction between N and I ground states can be unambiguously done only at the microscopic level: Calculations (see Ref. [6]) have shown that the N-I borderline is between $\varrho = 0.6$ (regular stack, i.e., equal distances between D and A) and $\varrho = 0.5$

(fully dimerized stack, i.e., a collection of noninteracting dimers).

[4] A. Girlando, F. Marzola, C. Pecile, and J. B. Torrance, J. Chem. Phys. **79**, 1075 (1983).

[5] A. Girlando, C. Pecile, and J. B. Torrance, Solid State Commun. **54**, 753 (1985).

[6] A. Girlando and A. Painelli, Phys. Rev. B **34**, 2131 (1986); A. Painelli and A. Girlando, *ibid.* **37**, 5748 (1988).

[7] S. Horiuchi, T. Hasegawa, and Y. Tokura, J. Phys. Soc. Jpn. **75**, 051016 (2006).

[8] A. Girlando, M. Masino, A. Painelli, N. Drichko, M. Dressel, A. Brillante, R. G. Della Valle, and E. Venuti, Phys. Rev. B **78**, 045103 (2008).

[9] G. D'Avino, M. Masino, A. Girlando, and A. Painelli, Phys. Rev. B **83**, 161105(R) (2011).

[10] A. Girlando, A. Painelli, S. A. Bewick, and Z. G. Soos, Synth. Metals **141**, 129 (2004).

[11] S. Horiuchi, R. Kumai, Y. Okimoto, and Y. Tokura, Chem. Phys. **325**, 78 (2006).

[12] Y. Iwasa, T. Koda, Y. Tokura, A. Kobayashi, N. Iwasawa, and G. Saito, Phys. Rev. B **42**, 2374 (1990).

[13] M. Buron-Le Cointe, M. H. Lemée-Cailleau, H. Cailleau, B. Toudic, A. Moréac, F. Moussa, C. Ayache, and N. Karl, Phys. Rev. B **68**, 064103 (2003).

[14] K. Imaeda, T. Enoki, H. Inokuchi, and G. Saito, Mol. Cryst. Liq. Cryst. **141**, 131 (1986).

[15] Y. Iwasa, T. Koda, S. Koshihara, Y. Tokura, and G. Saito, Mol. Cryst. Liq. Cryst. **216**, 195 (1992).

[16] CrysAlisPRO, Agilent Technologies Ltd., Version 1.171.37.35, release 13-08-2014, Yarnton, Oxfordshire, England.

[17] M. W. Schmidt, K. K. Baldridge, J. A. Boatz, S. T. Elbert, M. S. Gordon, J. H. Jensen, S. Koseki, N. Matsunaga, K. A. Nguyen, S. Su, T. L. Windus, M. Dupuis, and J. A. Montgomery, J. Comput. Chem. **14**, 1347 (1993).

[18] MOPAC2016, J. J. P. Stewart, Stewart Computational Chemistry, Colorado Springs, CO (2016); http://OpenMOPAC.net.

[19] See Supplemental Material at http://link.aps.org/supplemental/10.1103/PhysRevB.95.024101 for the shape of HOMO and LUMO, as obtained by DFT calculation, and for the computed vibrational frequencies of TMB and TMB^{+}.

[20] T. Kistenmacher, T. Emge, A. Bloch, and D. Cowan, Acta Cryst. B **38**, 1193 (1982).

[21] P. Hu, K. Du, F. Wei, H. Jiang, and C. Kloc, Crystal Growth Design **16**, 3019 (2016).

[22] R. Bozio, I. Zanon, A. Girlando, and C. Pecile, J. Chem. Soc. Faraday Trans. II **74**, 235 (1978).

[23] M. Meneghetti and C. Pecile, J. Chem. Phys. **84**, 4149 (1986).

[24] A. Morherr, S. Witt, A. Chernenkaya, J-P. Bäcker, G. Schönhense, M. Bolte, and C. Krellner, Physica B **496**, 98 (2016).

[25] M. Masino, A. Girlando, and Z. G. Soos, Chem. Phys. Lett. **369**, 428 (2003).

[26] A. Painelli and A. Girlando, J. Chem. Phys. **87**, 1705 (1987).

[27] A. Girlando and C. Pecile, Spectrochim. Acta A **29**, 1859 (1973).

[28] R. Bozio and C. Pecile, in *The Physics and Chemistry of Low Dimensional Solids, NATO ASI C56*, edited by L. Alcácer (Reidel, Dordrecht, Netherlands, 1980), p. 165.

[29] C. Pecile, A. Palnelli, and A. Girlando, Mol. Cryst. Liq. Cryst. **171**, 69 (1989).

[30] M. Hanfland, A. Brillante, A. Girlando, and K. Syassen, Phys. Rev. B **38**, 1456 (1988).

[31] M. Masino, A. Girlando, A. Brillante, R. G. Della Valle, and E. Venuti, Mater. Sci.-Poland **22**, 333 (2004).

[32] P. Ranzieri, M. Masino, A. Girlando, and M. H. Lemée-Cailleau, Phys. Rev. B **76**, 134115 (2007).

[33] A. Brillante, I. Bilotti, R. G. Della Valle, E. Venuti, and A. Girlando, Cryst. Eng. Commun. **10**, 937 (2008).

[34] M. Le Cointe, M. H. Lemée-Cailleau, H. Cailleau, B. Toudic, L. Toupet, G. Heger, F. Moussa, P. Schweiss, K. H. Kraft, and N. Karl, Phys. Rev. B **51**, 3374 (1995).

[35] S. N. Steinmann, C. Piemontesi, A. Delachat, and C. Corminboeuf, J. Chem. Theory Comput. **8**, 1629 (2012)

[36] J. Nyman, O. S. Pundyke, and G. M. Day, Phys. Chem. Chem. Phys. **18**, 15828 (2016).

[37] Program STRCONVERT at the Bilbao Crystallographic server, http://www.cryst.ehu.es/index.html.

[38] Z. G. Soos and A. Painelli, Phys. Rev. B **75**, 155119 (2007).

[39] V. Oison, C. Katan, and C. Koenig, J. Phys. Chem. A **105**, 4300 (2001).